

Terahertz Polarizers Based on 2D $\text{Ti}_3\text{C}_2\text{T}_z$ MXene: Spin Cast from Aqueous Suspensions

Guangjiang Li, Kiana Montazeri, Mostafa K. Ismail, Michel W. Barsoum, Bahram Nabet, and Lyubov V. Titova*

Herein, the fabrication of terahertz (THz) polarizers is reported on by simply spin casting two-dimensional (2D) MXene $\text{Ti}_3\text{C}_2\text{T}_z$ nanosheets on a photolithographically patterned THz-transparent substrate and subsequent immersion in acetone. Lines 30 nm-thick and 10–20 μm wide result in electric field (E) extinction ratios (ER) of up to 3 dB, or power ER of up to 6 dB. Simulations show the possibility of achieving ER beyond 16 dB, or power ER higher than 32 dB by increasing the thickness of the MXene lines to 1.5–2 μm and optimizing the metasurface patterns. The $\text{Ti}_3\text{C}_2\text{T}_z$ nanosheets are solution-processed and can be deposited on a variety of substrates, including flexible ones. Once encapsulated, chemically stable THz polarizers, that combine high performance and low production costs, can be readily manufactured, with characteristics that compare favorably with the much more involved metallic wire grid polarizers, including gold and tungsten. Moreover, recent demonstration of dynamic tunability of $\text{Ti}_3\text{C}_2\text{T}_z$ THz conductivity by ultrafast optical pulses opens the possibility of using MXene wire-grids in high-speed THz modulators.

applications require other active/passive THz optical components, such as linear polarizers for which high extinction ratios (ERs) and low insertion losses (ILs) are critical parameters for analyzing the polarization properties of THz signals.^[6] Currently, commercially available THz polarizers are either free-standing or supported metallic wire grids. Free-standing polarizers have high power ERs (≈ 20 – 40 dB) and low ILs, but are expensive and fragile.^[6] Substrate-supported metal, typically Al, wire-grid polarizers are more robust and can be produced by photolithography,^[7,8] hot embossing,^[9] etching,^[10] or nanoimprinting.^[11] Some of these have recently been successfully demonstrated on flexible substrates, an important step toward conformable THz devices.^[12]

1. Introduction

Over the past two decades, rapid improvement in tabletop sources of terahertz (THz) radiation has inspired growth in THz technology applications for materials characterization, pharmaceuticals, imaging, communications, and sensing, among others.^[1–5] In addition to reliable sources and detectors, these


Inherent anisotropic conductivity of 1D nanostructures such as semiconducting or metallic nanowires, or carbon nanotubes, has motivated efforts to design THz polarizers based on highly aligned nanowire or nanotube arrays.^[13–17] These structures achieve high-performance characteristics, and, in the case of semiconductor nanowires, are dynamically switchable.^[17] However, achieving high degrees of alignment of nanowires or nanotubes over macroscopic regions remains challenging.

MXenes, a new class of solution-processable 2D materials with conductivities that can rival those of some conventional metals, are poised to become a material of choice for a number of THz photonic device applications.^[18–32] Here, we propose broadband THz polarizers based on a hydrophilic 2D MXene with metallic conductivity, $\text{Ti}_3\text{C}_2\text{T}_z$. The latter is obtained by selectively etching, the Al layers from the parent Ti_3AlC_2 MAX phase and replacing them with O, OH, and/or F-terminations, labeled as T_z in the chemical formula.^[18,19] Discovered 10 years ago, MXenes combine metallic conductivity, excellent mechanical properties, and ease of processing owing to the hydrophilicity of their surface termination groups. These 2D solids have already inspired a host of applications that leverage their high electrical conductivities (≈ 1000 – $10\,000$ ($\Omega\text{ cm}$)⁻¹) such as transparent flexible conductors, THz detectors, and electromagnetic interference (EMI) shielding in the gigahertz (GHz) and THz frequency ranges.^[20–32] In fact, $\text{Ti}_3\text{C}_2\text{T}_z$ films have been shown to exceed EMI shielding efficiency of carbon nanostructures and their composites, and perform comparably to copper (Cu) and silver (Ag), all while being significantly more lightweight.^[29]

G. Li, Prof. L. V. Titova
Department of Physics
Worcester Polytechnic Institute
Worcester, MA 01609, USA
E-mail: ltitova@wpi.edu

K. Montazeri, M. K. Ismail, Prof. B. Nabet
Electrical and Computer Engineering Department
Drexel University
Philadelphia, PA 19104, USA

Prof. M. W. Barsoum
Department of Materials Science and Engineering
Drexel University
Philadelphia, PA 19104, USA

 The ORCID identification number(s) for the author(s) of this article can be found under <https://doi.org/10.1002/adpr.202000084>.

© 2020 The Authors. Published by Wiley-VCH GmbH. This is an open access article under the terms of the Creative Commons Attribution License, which permits use, distribution and reproduction in any medium, provided the original work is properly cited.

DOI: 10.1002/adpr.202000084

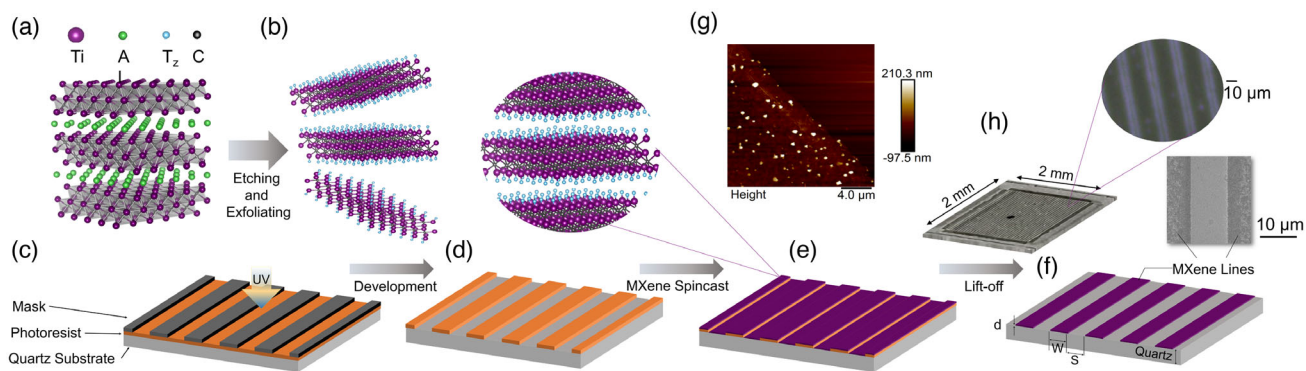


Figure 1. Fabrication process of MXene wire-grid polarizer. a,b) Preparation of MXene colloidal suspension. c,d) Conventional photolithography is performed resulting in exposed areas for striations. e) MXene aqueous colloidal suspension is spin-coated, and f) lifted off by immersion in acetone. g) AFM of a striation edge. h) Optical image of the final device and SEM close-up of striations.

MXene patterning had previously been conducted using laser printers,^[33] or microcontact printing techniques,^[34] with large feature sizes. We have recently shown that MXene photodetectors that outperform more standard gold-based ones can be fabricated by simply spin-coating transparent Ti_3C_2 -based MXene electrodes from aqueous suspensions onto a substrate patterned with a photoresist, followed by immersion in acetone.^[35] Here, we demonstrate that this approach is also applicable to the photonic devices not only in the visible, but also in the THz range, where it can be used to deposit polarizer structures on a variety of substrates, paving the way to MXene-based THz photonics. In a proof of principle, here we experimentally demonstrate that very thin (≈ 30 nm), $10\text{--}20\ \mu\text{m}$ wide striations of spin-coated $\text{Ti}_3\text{C}_2\text{T}_z$, consisting of overlapping nanosheets that are $1\text{--}3\ \mu\text{m}$ in lateral dimensions, exhibit excellent polarization properties over the $0.3\text{--}2.0$ THz spectral range, with electric field ERs of up to 3 dB, corresponding to power ERs of 6 dB. Using simulations, we further show that increasing the line thicknesses to $1.5\text{--}2\ \mu\text{m}$, and optimizing the periods and fill factors of the periodic structures, can increase ER to >16 dB for the electric field or >32 dB for the power while maintaining low IILs.

2. Experimental Section

The MXene polarizer devices ($2 \times 2\ \text{mm}^2$) composed of parallel line patterns were deposited on quartz substrates using conventional photolithography and a simple fabrication process. Performance of the devices was evaluated using a standard THz time-domain spectroscopy (THz-TDS) experiment, accompanied by simulations using COMSOL Multiphysics software.

The device fabrication process is shown schematically in **Figure 1**, where first the Ti_3AlC_2 MAX phase (**Figure 1a**) was etched and delaminated to obtain a colloidal aqueous suspension of $\text{Ti}_3\text{C}_2\text{T}_z$ single or few flakes (**Figure 1b**), as described in detail in Supporting Information. Several patterns of striations, with various widths ($w = 10$ and $20\ \mu\text{m}$), separated by spaces ($s = 10, 30$, and $40\ \mu\text{m}$), were formed using photoresist and conventional contact lithography on quartz substrates (**Figure 1c**) and developed (**Figure 1d**). A detailed description of the photolithography procedure is shown in **Figure S1** and **S2**, Supporting Information.

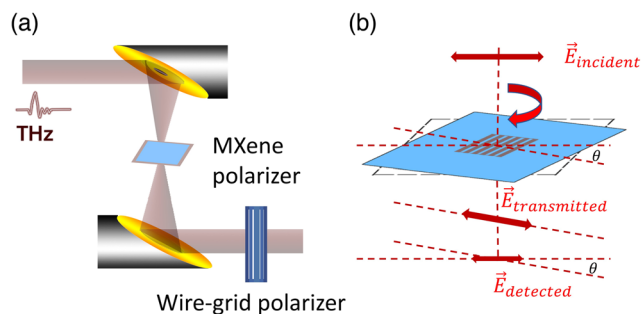


Figure 2. a) Schematic diagram of experiment: incident THz pulse is focused to a $\approx 1.5\ \text{mm}$ spot on the polarizer using an off-axis polarizer; another polarizer collects the transmitted pulse, which goes through a commercial wire-grid polarizer before being detected. b) A linearly polarized THz pulse is normally incident on a MXene polarizer, which can be rotated around the normal; only a component that is parallel to the incident pulse polarization is detected.

The MXene colloidal suspension was then spin cast on the substrate (**Figure 1e**). Lastly, the photoresist was removed by immersing the device in acetone (**Figure 1f**) in a conventional lift-off process, leaving MXene striations covering a $2 \times 2\ \text{mm}^2$ area (**Figure 1g**). The thicknesses of the resulting lines were measured by atomic force microscopy (AFM) using a tapping mode of the probe at ambient conditions and was found to be ≈ 30 nm (**Figure 1h**). The sharpness of the edges, seen in AFM and scanning electron microscope (SEM) images (**Figure 1i**), indicate that the resolution of this method is primarily limited by lithography, as discussed in more detail in Supporting Information. The lift-off process is performed at room temperature (RT) and under ambient conditions, and does not require high vacuum, high-temperature deposition chambers, nor plasma (dry) etching capabilities. It is also compatible with common microfabrication techniques including photonic integrated circuits and silicon photonics.

We evaluated the performance of the polarizers using a conventional THz-TDS setup (**Figure 2a**). THz pulses were generated by the optical rectification of 100 fs, 800 nm pulses from a 1 kHz repetition rate amplified Ti:S laser (Coherent Libra) in a 1 mm-thick [110] ZnTe crystal. The THz pulses were

focused to a ≈ 1.5 mm spot on a polarizer device using an off-axis parabolic mirror. The transmitted pulses were collected by another off-axis parabolic mirror and coherently detected by free-space electro-optic sampling in a second 1 mm-thick [110] ZnTe crystal (Figure 2a). The wire-grid polarizer (Microtech Instruments; field extinction ratio of 0.01) ensured that only the component of the transmitted pulse that was parallel to the incident pulse polarization was detected. The orientations of the samples were varied by rotating the samples by an angle θ (Figure 2b).

An example reference THz pulse that propagated through air without the sample in its path, along with the pulses transmitted through the quartz substrate and through one of the polarizer structures with lines oriented along the polarization of the

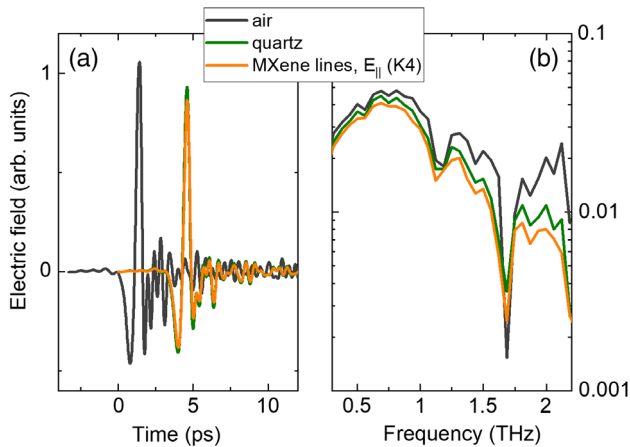


Figure 3. a) Reference THz waveform (transmitted through air), and THz waveforms transmitted through quartz substrate and through one of the polarizer devices (K5) with lines oriented along incident THz polarization. b) Corresponding THz amplitude as a function of frequency. Dips in frequency are due to absorption by water vapor.

THz probe pulse, is shown in Figure 3a. The corresponding THz amplitude is shown in Figure 3b. The ≈ 1 mm-thick quartz substrate with a refractive index of 2.156 at 1 THz^[36] introduces a significant delay in the arrival of the probe pulse, and attenuates the transmitted pulse due to reflection losses. The IL due to a quartz substrate, defined as, $IL_{\text{quartz}} = -10 \log(\frac{E_{\text{quartz}}}{E_{\text{ref}}})$ is ≈ 0.6 dB at 1 THz, as shown in Figure S3, Supporting Information. For future applications, THz-transparent flexible substrates with lower refractive indices will be used to minimize ILs. In the following analysis, we focus on the IL introduced by the MXene structures alone, treating the THz pulses transmitted through the quartz substrate as a reference. Dips in the THz amplitudes at ≈ 1.15 and ≈ 1.7 THz are due to strong absorption of THz radiation by water vapor in ambient air, which results in a reduction of the signal- to-noise ratio in the vicinity of those frequencies.

Finite-difference time-domain (FDTD) simulations of our $\text{Ti}_3\text{C}_2\text{T}_z$ polarizer performance at 1 THz as a function of period ($w + s$), fill factor ($w/(w + s)$), and line thicknesses were conducted using the RF module of the commercial solver COMSOL Multiphysics, as described in more detail in Figure S4, Supporting Information. The properties of $\text{Ti}_3\text{C}_2\text{T}_z$ in the THz range were parameterized using a Drude–Smith model^[37,38] following previous reports.^[31,32,39] To model the polarizers, we assumed a carrier density of $4 \times 10^{20} \text{ cm}^{-3}$, a scattering time of 40 fs, and a Drude–Smith c-parameter of -0.75 , representing the effect of $\text{Ti}_3\text{C}_2\text{T}_z$ nanoflake boundaries and disorder on the long-range electron transport. Details of the Drude–Smith analysis are provided in Figure S5, Supporting Information.

3. Results and Discussion

Rotation of the polarizer structure about the normal through an angle θ (Figure 2) results in a characteristic Malus's law $\cos^2(\theta)$ dependence, as shown in Figure 4, which plots the peak

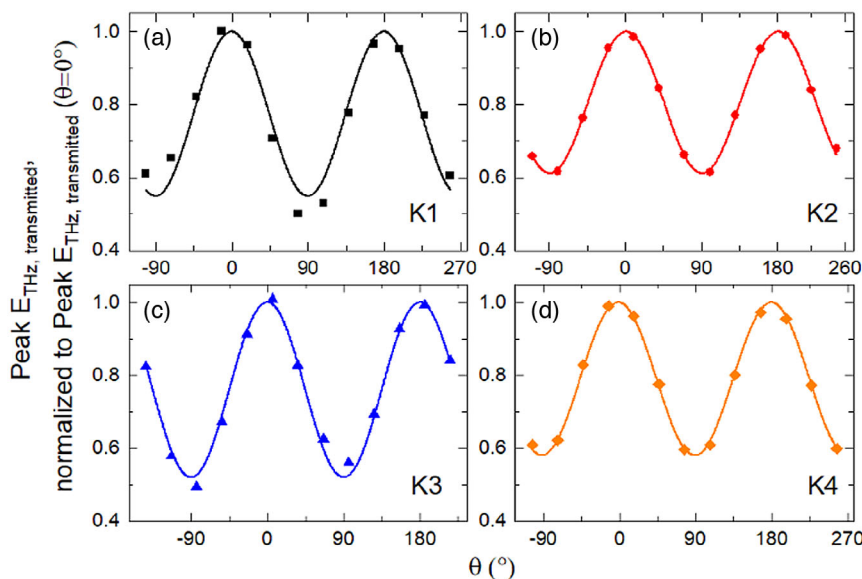


Figure 4. Peak of transmitted THz pulses, normalized to its value for $\theta = 0^\circ$, as a function of θ , for polarizer structures a) K1, b) K2, c) K3, and d) K4. Symbols show experimental data, and lines—Malus's law fits.

of the transmitted pulse as a function of θ for four different polarizer structures K1 ($w = 10 \mu\text{m}$, $s = 10 \mu\text{m}$), K2 ($w = 10 \mu\text{m}$, $s = 30 \mu\text{m}$), K3 ($w = 20 \mu\text{m}$, $s = 10 \mu\text{m}$), and K4 ($w = 20 \mu\text{m}$, $s = 40 \mu\text{m}$). The resulting peak degrees of polarization, defined as $\frac{E_{\perp} - E_{\parallel}}{E_{\perp} + E_{\parallel}}$, range from $\approx 30\%$ for K1 and K3, down to 27% for K4 and 24% for K2. The entire time domain waveforms for the electric field of the incident THz pulse parallel and perpendicular to the polarizer lines, for all four structures, are shown in **Figure 5**, where the reference THz pulses transmitted through the quartz substrate are also shown and so labelled. The frequency-resolved THz amplitudes of the waveforms in **Figure 5** are then used to calculate the electric field ERs ($ER = 10 \log(\frac{E_{\perp}}{E_{\parallel}})$) and ILs, $IL = -10 \log(\frac{E_{\perp}}{E_{\parallel}})$, which are shown in **Figure 6** as a function of frequency. While the demonstrated ER values are significantly lower than those for commercially available structures ($10\text{--}20 \text{ dB}$ for electric field, or $20\text{--}40 \text{ dB}$ for power), we stress here that the thicknesses of the MXene lines in the polarizers studied here were only $\approx 30 \text{ nm}$, compared with $\approx 20\text{--}40 \mu\text{m}$ -thick metal wires that are typically used in commercial wire-grids. In fact, for the best performing structure (K1), ER is only \approx a factor of 2 lower than that demonstrated for single layer, $2 \mu\text{m}$ -thick carbon nanotube polarizers.^[13,14] Comparing the performance of the four structures, we observe that the narrower lines ($10 \text{ vs } 20 \mu\text{m}$) and narrow gaps ($10 \mu\text{m}$) yield the best compromise between ER and IL. The wider lines with the same gap (K3) result in a higher area filling fraction ($2/3 \text{ vs } 1/2$); IL increases without gain in ER. For the lower filling fractions, ER is reduced.

To further explore how the MXene polarizer performance can be optimized by geometry, such as varying the period, filling fraction, or line thicknesses, we conducted FDTD simulations at a frequency 1 THz (**Figure 7**). For periods of $20 \mu\text{m}$, filling fractions of 0.5 and line thicknesses of 30 nm —corresponding to the K1 polarizer geometry—our simulations yield ER of 2.6 dB and an IL of 0.6 dB (**Figure 7a,b**), in good agreement with our

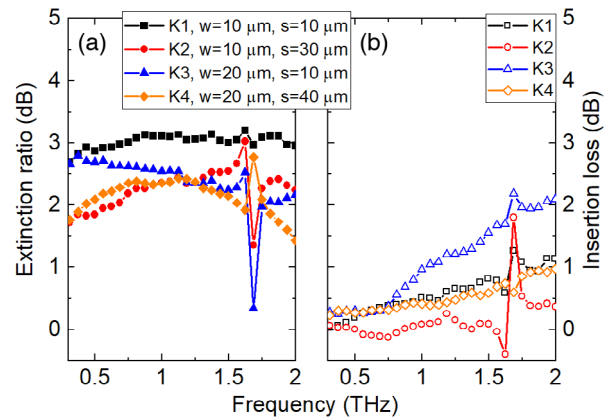


Figure 6. a) Electric field extinction ratios, and b) insertion losses for four THz polarizer devices.

experimental results (**Figure 6** and **4**). We attribute the small deviations of the experimental results from the simulations to inhomogeneities in the fabricated devices.

As expected, we find that increasing the filling factor by increasing the line width w , while keeping the period constant, increases the ILs. The ER increases up to a filling fraction of $\approx 0.5\text{--}0.7$ (**Figure 7**). If the filling fraction is fixed at the near optimal value of 0.7 , we find that narrower lines are more desirable, as they minimize ILs alongside a modest improvement in ERs. Finally, we find that increasing the line thickness dramatically improves polarizer performance, with electric field ER saturating at $\approx 16 \text{ dB}$ for a thickness of $\approx 1 \mu\text{m}$ (**Figure 7e**). The optimal MXene polarizer thickness agrees well with a calculated $\text{Ti}_3\text{C}_2\text{T}_z$ skin depth at 1 THz , $\delta = \sqrt{\frac{2}{\omega\mu_0\sigma}} \approx 0.9 \mu\text{m}$, where μ_0 is the vacuum permeability, $\omega/2\pi = 1 \text{ THz}$, $\sigma(1 \text{ THz}) \approx 5000 (\Omega \text{ cm})^{-1}$ (**Figure S5**, Supporting Information).

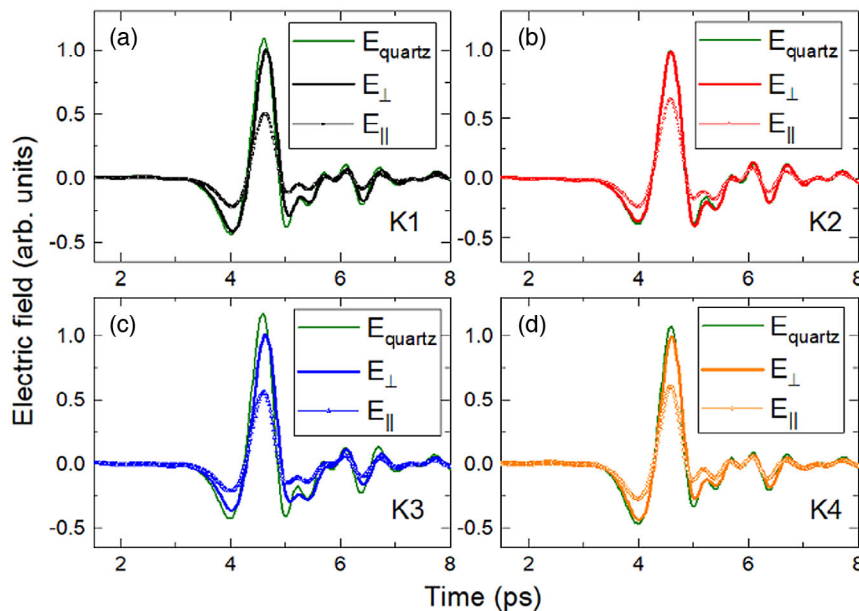


Figure 5. Transmitted THz pulses in time domain for incident THz pulse polarization parallel and perpendicular to the lines, for polarizer structures a) K1, b) K2, c) K3, and d) K4. Reference THz pulses transmitted through the quartz substrate are also shown.

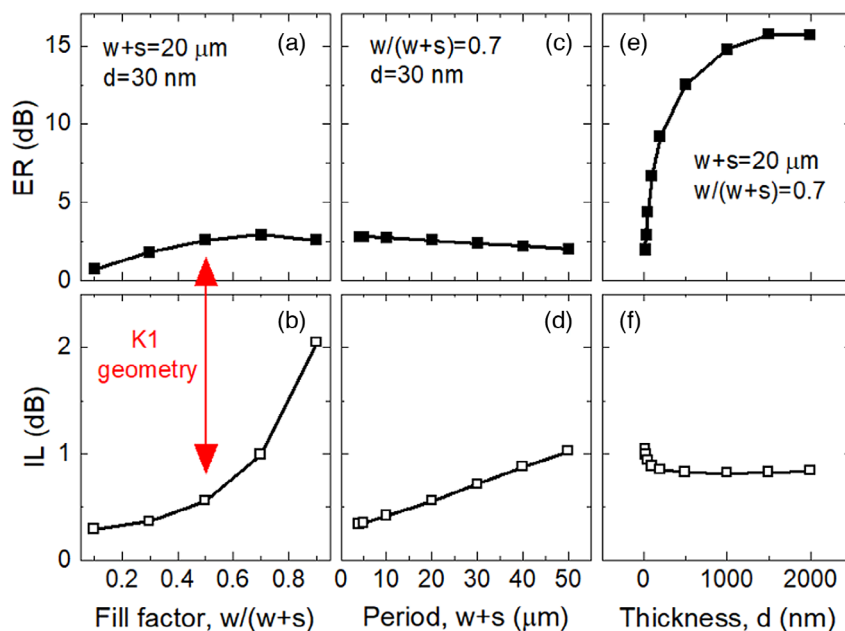


Figure 7. a,c,e) Simulated ER and b,d,f) IL at 1 THz as a function of a,b) fill factor, c,d) period, and e,f) thickness. Parameters that were fixed in a simulation are given in the top panels (a,d,e).

In conclusion, herein we demonstrated proof of concept of a THz polarizer based on parallel lines of overlapping $\text{Ti}_3\text{C}_2\text{T}_z$ nanosheets that are solution-processed and can be deposited on a variety of substrates. Lines only 30 nm-thick yield electric field ERs of up to 3 dB, or power ERs of up to 6 dB. Simulations show that ERs can be increased up to >16 dB for electric fields (Figure 7e), or >32 dB for power by increasing the line thickness to 1.5–2 μm , with line widths of 10 μm or less, and area filling fractions in the 0.5–0.7 range giving the optimal results. The projected performance is comparable to commercial polarizers at a fraction of the cost and thickness. We propose to increase the thickness of the optimized devices by stacking multiple layers of MXene lines on THz-transparent, flexible substrates such as PDMS or TPX, which can also serve to encapsulate the MXene structures to prevent their oxidation. This will result in flexible, free-standing thin layers that can be stacked to achieve high extinction ratios while maintaining low IL, low weight, and chemical stability. Moreover, possibility of dynamical control over $\text{Ti}_3\text{C}_2\text{T}_z$ THz conductivity has been recently demonstrated, suggesting that dynamically tunable polarizers for high-speed THz devices may be achieved.^[31] The same simple fabrication process, spin casting from an aqueous solution, can be applied in the future to other MXenes, resulting in a variety of novel THz photonic devices.

Supporting Information

Supporting Information is available from the Wiley Online Library or from the author.

Acknowledgements

G.L. and K.M. contributed equally to this work. G.L. and L.V.T. thank Worcester Polytechnic Institute for financial support via Transformative

Research and Innovation, Accelerating Discovery (TRIAD) seed grant. This work was funded by the Division of Materials Research of NSF (DMR 1740795). This work was conducted in part at Singh Center for Nanotechnology of the University of Pennsylvania through a grant to NanoGrass Photonics LLC. Singh Center is supported by the NSF National Nanotechnology Coordinated Infrastructure Program under grant NNCI-1542153.

Conflict of Interest

The authors declare no conflict of interest.

Keywords

MXene, polarizer, terahertz, Ti_3C_2

Received: October 1, 2020
Published online: November 17, 2020

- [1] P. U. Jepsen, D. G. Cooke, M. Koch, *Laser Photonics Rev.* **2011**, 5, 124.
- [2] T. Kürner, S. Priebe, *J. Infrared Millim. Terahertz Waves* **2014**, 35, 53.
- [3] J. Ma, R. Shrestha, J. Adelberg, C.-Y. Yeh, Z. Hossain, E. Knightly, J. M. Jornet, D. M. Mittleman, *Nature* **2018**, 563, 89.
- [4] D. M. Mittleman, *Nat. Photonics* **2013**, 7, 666.
- [5] M. Tonouchi, *Nat. Photonics* **2007**, 1, 97.
- [6] F. Yan, C. Yu, H. Park, E. P. J. Parrott, E. Pickwell-MacPherson, *J. Infrared Millim. Terahertz Waves* **2013**, 34, 489.
- [7] I. Yamada, K. Takano, M. Hangyo, M. Saito, W. Watanabe, *Opt. Lett.* **2009**, 34, 274.
- [8] Z. Huang, E. P. J. Parrott, H. Park, H. P. Chan, E. Pickwell-MacPherson, *Opt. Lett.* **2014**, 39, 793.
- [9] A. Partanen, J. Väyrynen, S. Hassinen, H. Tuovinen, J. Mutanen, T. Itkonen, P. Silfsten, P. Pääkkönen, M. Kuittinen, K. Mönkkönen, T. Venäläinen, *Appl. Opt.* **2012**, 51, 8360.

- [10] L. Y. Deng, J. H. Teng, L. Zhang, Q. Y. Wu, H. Liu, X. H. Zhang, S. J. Chua, *Appl. Phys. Lett.* **2012**, *101*, 011101.
- [11] K. Takano, H. Yokoyama, A. Ichii, I. Morimoto, M. Hangyo, *Opt. Lett.* **2011**, *36*, 2665.
- [12] A. Ferraro, D. C. Zografopoulos, M. Missori, M. Peccianti, R. Caputo, R. Beccherelli, *Opt. Lett.* **2016**, *41*, 2009.
- [13] L. Ren, C. L. Pint, T. Arikawa, K. Takeya, I. Kawayama, M. Tonouchi, R. H. Hauge, J. Kono, *Nano Lett.* **2012**, *12*, 787.
- [14] L. Ren, C. L. Pint, L. G. Booshehri, W. D. Rice, X. Wang, D. J. Hilton, K. Takeya, I. Kawayama, M. Tonouchi, R. H. Hauge, J. Kono, Carbon Nanotube Terahertz Polarizer, *Nano Lett.* **2009**, *9*, 2610.
- [15] J. Kyoung, E. Y. Jang, M. D. Lima, H.-R. Park, R. O. Robles, X. Lepró, Y. H. Kim, R. H. Baughman, D.-S. Kim, *Nano Lett.* **2011**, *11*, 4227.
- [16] W. Xiang, X. Huang, D. Li, Q. Zhou, H. Guo, J. Li, *Opt. Lett.* **2020**, *45*, 1978.
- [17] S. A. Baig, J. L. Boland, D. A. Damry, H. H. Tan, C. Jagadish, H. J. Joyce, M. B. Johnston, *Nano Lett.* **2017**, *17*, 2603.
- [18] M. Naguib, M. Kurtoglu, V. Presser, J. Lu, J. Niu, M. Heon, L. Hultman, Y. Gogotsi, M. W. Barsoum, *Adv. Mater.* **2011**, *23*, 4248.
- [19] M. Naguib, O. Mashtalir, J. Carle, J. Lu, L. Hultman, Y. Gogotsi, M. W. Barsoum, *ACS Nano* **2012**, *6*, 1322.
- [20] M. Naguib, O. Mashtalir, J. Carle, V. Presser, J. Lu, L. Hultman, Y. Gogotsi, M. W. Barsoum, *ACS Nano* **2012**, *6*, 1322.
- [21] L. Verger, V. Natu, M. Carey, M. W. Barsoum, *Trends Chem.* **2019**, *1*, 656.
- [22] B. Anasori, Y. Xie, M. Beidaghi, J. Lu, B. C. Hosler, L. Hultman, P. R. C. Kent, Y. Gogotsi, M. W. Barsoum, *ACS Nano* **2015**, *9*, 9507.
- [23] M. Khazaei, A. Mishra, N. S. Venkataramanan, A. K. Singh, S. Yunoki, *Curr. Opin. Solid State Mater. Sci.* **2019**, *23*, 164.
- [24] M. Naguib, V. N. Mochalin, M. W. Barsoum, Y. Gogotsi, *Adv. Mater.* **2014**, *26*, 992.
- [25] G. Choi, F. Shahzad, Y. M. Bahk, Y. M. Jhon, H. Park, M. Alhabeab, B. Anasori, D. S. Kim, C. M. Koo, Y. Gogotsi, M. Seo, *Adv. Opt. Mater.* **2018**, *6*, 1701076.
- [26] A. D. Dillon, M. J. Ghidui, A. L. Krick, J. Griggs, S. J. May, Y. Gogotsi, M. W. Barsoum, A. T. Fafarman, *Adv. Funct. Mater.* **2016**, *26*, 4162.
- [27] W. Feng, H. Luo, Y. Wang, S. Zeng, L. Deng, X. Zhou, H. Zhang, S. Peng, *RSC Adv.* **2018**, *8*, 2398.
- [28] Y. I. Jhon, M. Seo, Y. M. Jhon, *Nanoscale* **2018**, *10*, 69.
- [29] F. Shahzad, M. Alhabeab, C. B. Hatter, B. Anasori, S. Man Hong, C. M. Koo, Y. Gogotsi, *Science* **2016**, *353*, 1137.
- [30] C. Zhang, B. Anasori, A. Seral-Ascaso, S. H. Park, N. McEvoy, A. Shmeliov, G. S. Duesberg, J. N. Coleman, Y. Gogotsi, V. Nicolosi, *Adv. Mater.* **2017**, *29*, 1702678.
- [31] G. Li, N. Amer, H. A. Hafez, S. Huang, D. Turchinovich, V. N. Mochalin, F. A. Hegmann, L. V. Titova, *Nano Lett.* **2019**, *20*, 636.
- [32] G. Li, K. Kushnir, Y. Dong, S. Chertopalov, A. M. Rao, V. N. Mochalin, R. Podila, L. V. Titova, *2D Mater.* **2018**, *5*, 035043.
- [33] H. Hu, T. Hua, *J. Mater. Chem. A* **2017**, *5*, 19639.
- [34] B. Xu, M. Zhu, W. Zhang, X. Zhen, Z. Pei, Q. Xue, C. Zhi, P. Shi, *Adv. Mater.* **2016**, *28*, 3333.
- [35] K. Montazeri, M. Currie, L. Verger, P. Dianat, M. W. Barsoum, B. Nabet, *Adv. Mater.* **2019**, *31*, 1903271.
- [36] D. Grischkowsky, S. Keiding, M. van Exter, C. Fattinger, *J. Opt. Soc. Am. B* **1990**, *7*, 2006.
- [37] N. Smith, *Phys. Rev. B* **2001**, *64*.
- [38] T. L. Cocker, D. Baillie, M. Buruma, L. V. Titova, R. D. Sydora, F. Marsiglio, F. A. Hegmann, *Phys. Rev. B* **2017**, *96*, 205439.
- [39] G. Li, V. Natu, T. Shi, M. W. Barsoum, L. V. Titova, *ACS Appl. Energy Mater.* **2020**.